Taking large-eddy simulation of wall-bounded flows to higher Reynolds numbers by use of anisotropy-resolving subgrid models

Matteo Montecchia,* Geert Brethouwer, Arne V. Johansson, and Stefan Wallin
Linné FLOW Centre, KTH Mechanics, SE-100 44 Stockholm, Sweden
(Received 28 April 2016; published 3 March 2017)

Properly resolved large-eddy simulations of wall-bounded high Reynolds number flows using standard subgrid-scale (SGS) models requires high spatial and temporal resolution. We have shown that a more elaborate SGS model taking into account the SGS Reynolds stress anisotropies can relax the requirement for the number of grid points by at least an order of magnitude for the same accuracy. This was shown by applying the recently developed explicit algebraic subgrid-scale model (EAM) [Marstorp *et al.*, J. Fluid Mech. **639**, 403 (2009)] to fully developed high Reynolds number channel flows with friction Reynolds numbers of 550, 2000, and 5200. The near-wall region is fully resolved, i.e., no explicit wall modeling or wall functions are applied. A dynamic procedure adjusts the model at the wall for both low and high Reynolds numbers. The resolution is reduced, from the typically recommended 50 and 15 wall units in the stream- and spanwise directions respectively, by up to a factor of 5 in each direction. It was shown by comparison with direct numerical simulations that the EAM is much less sensitive to reduced resolution than the dynamic Smagorinsky model. Skin friction coefficients, mean flow profiles, and Reynolds stresses are better predicted by the EAM for a given resolution. Even the notorious overprediction of the streamwise fluctuation intensity typically seen in poorly resolved LES is significantly reduced when EAM is used on coarse grids. The improved prediction is due to the capability of the EAM to capture the SGS anisotropy, which becomes significant close to the wall.

DOI: 10.1103/PhysRevFluids.2.034601

I. INTRODUCTION

Large-eddy simulation (LES) is nowadays regularly applied in academic research and more and more in engineering. However, LES of moderate or high Reynolds number turbulent wall-bounded flows still poses strong modeling and computational challenges stemming mainly from the representation of the strongly anisotropic near-wall structures that are fundamental for momentum transfer. The simplest approach is to largely resolve these structures, but the computational costs of such a wall-resolved LES tend to become extreme at high Reynolds numbers since near-wall structures scale in viscous wall units [1]. For example, a wall-resolved LES of fully developed turbulent channel flow, at a friction Reynolds number $\mathrm{Re}_\tau = u_\tau h/\nu = 5200$ and the same domain size and wall-normal resolution as those of the LES presented later, would require 1.8 billion grid points if the recommended streamwise and spanwise grid spacings in viscous wall units of $\Delta x^+ = 50$ and $\Delta z^+ = 15$, respectively, given by [2] are used. Here, u_τ is the friction velocity and h the channel half-height. Such a large-scale LES would evidently be impractical for engineering.

To reduce computational costs of wall-bounded flow, alternatives to wall-resolved LES have been proposed. Common alternatives used in engineering circumvent the need of resolving wall structures or even all boundary layer structures by using a Reynolds-averaged Navier-Stokes (RANS) model for these, as in hybrid RANS/LES and detached-eddy simulation (DES), or solving simplified governing equations near the wall, as in wall-modeled LES (WMLES). Such approaches, that only resolve large eddies away from the wall and consequently have greatly reduced computational demands, have been reviewed in Refs. [3–8]. A wide classification of the different hybrid RANS/LES techniques, with additional test cases, has been also provided in Ref. [9]. Basically, the resolution requirement

*matteomo@mech.kth.se

for WMLES in the stream- and spanwise directions scales with the boundary layer thickness. The improved delayed detached-eddy simulation (IDDES) [10,11] acts as a WMLES, if the large scale wall turbulence is sufficiently resolved, and can predict turbulent channel flow on a very coarse grid (no more than a million grid points) with Re_τ ranging from 400 to 18 000. The resolution requirement is almost independent of the Reynolds number, and WMLES cannot be replaced by wall-resolved LES for high Reynolds number boundary layers in the near future.

However, these methods have disadvantages; for instance, coupling the wall-modeled and LES parts with the interface within the boundary layer poses problems, and occasionally there is a mismatch between the mean velocity in these two parts [5,8]. Using different numerical methods for stability reasons and turbulence models for the inner and outer parts as done in some hybrid and DES methods adds to their complexity.

These drawbacks are mostly avoided in wall-resolved LES, simply called LES from now on, which therefore still has a clear appeal. The question addressed in this paper is whether a more physically correct SGS stress model can reduce computational demands of LES of wall-bounded flows. To this end, we perform LES of quite high Re_τ fully developed turbulent channel flow at reasonably fine to coarse resolutions with the popular dynamic Smagorinsky model (DSM) [12] and the more advanced explicit algebraic SGS stress model (EAM). The recent availability of high-quality direct numerical simulation (DNS) data of turbulent channel flow at high Re_τ [13] makes a careful validation of the LES possible.

The EAM is based on algebraic approximations of the modeled transport equations of SGS stresses [14] and aims to better describe SGS anisotropy, which is strong near the walls, than standard eddy viscosity models through a more complete description of the SGS physics. LES with the EAM has been applied to channel flow and more complex flows with separation with good results [14,15], and recently it was extended to SGS passive scalar transport [16].

Rasam *et al.* [17] validated the EAM, the dynamic Smagorinsky model, and a high-pass filtered model in LES of channel flow at $\mathrm{Re}_\tau = 934$ at five resolutions ranging from reasonable to coarse, and found that LES with the EAM is much less sensitive to grid resolutions and agrees better with DNS than LES with the other models. This motivated us to use the EAM also in the present study. Kremer and Bogey [18] recently validated LES of channel flow using relaxation filtering at $\mathrm{Re}_\tau = 300$ and various resolutions and at $\mathrm{Re}_\tau = 600$ and 960 at one resolution, but in all cases the resolution was $\Delta x^+ \leqslant 45$ and $\Delta z^+ \leqslant 15$. Piomelli, Rouhi, and Geurts [19] proposed a SGS model in which the model length scale is related to the turbulence activity instead of the grid and applied it in LES of channel flow at $\mathrm{Re}_\tau = 950$ and 2000. Even at a coarse resolution of $\Delta x^+ \simeq 120$ and $\Delta z^+ \simeq 60$ fair agreement with DNS was observed.

In this paper, we present LES of channel flow at $\mathrm{Re}_\tau = 550$, 2000, and 5200 at various resolutions, and show that LES with the EAM gives fair to good results for, e.g., the mean velocity profiles and skin friction coefficient for resolutions as low as $\Delta x^+ \simeq 250$ and $\Delta z^+ \simeq 100$, while the LES with the dynamic Smagorinsky model then gives worse results. The LES with coarse resolution has 53 million grid points at $\mathrm{Re}_\tau = 5200$, which is much more acceptable than the 1.8 billion mentioned above. This shows that by improving SGS stress models we can drastically reduce computational costs of wall flow LES and make it a more attractive option for research and design.

The main goal of this work is to present a comparison between a standard model used for LES applications, i.e., the DSM, and the novel EAM, at significantly high Reynolds numbers using a (very) coarse resolution. The importance and the contribution of the SGS anisotropy-resolving part will be analyzed in detail.

In the next sections some LES notations will be presented, together with the description of the EAM. Thereafter, we present LES results for one-point statistics and spectra.

II. LARGE-EDDY SIMULATION (LES) AND SGS MODELS

The governing equations in Large-eddy simulation (LES) are here represented by the filtered, nondimensional Navier-Stokes equations, which for an incompressible flow read (where $\widetilde{\cdot}$ denotes

filtered quantity) [20]

$$\frac{\partial \widetilde{u}_i}{\partial x_i} = 0, \quad \frac{\partial \widetilde{u}_i}{\partial t} + \frac{\partial \widetilde{u}_i \widetilde{u}_j}{\partial x_j} = -\frac{\partial \widetilde{p}}{\partial x_i} + \frac{1}{\mathrm{Re}} \frac{\partial^2 \widetilde{u}_i}{\partial x_j \partial x_j} - \frac{\partial \tau_{ij}}{\partial x_j}. \tag{1}$$

Here τ_{ij} is the subgrid-scale stress tensor, defined as

$$\tau_{ij} = \widetilde{u_i u_j} - \widetilde{u}_i \widetilde{u}_j, \tag{2}$$

and it represents an unknown part in the filtered equations that needs to be modeled.

A. Explicit algebraic SGS model (EAM)

Anisotropic effects of turbulence persist down to relatively small scales in many flow situations, notably in the near-wall region, near flow separation, and in flows subject to rotation or strong curvature. For typical resolutions used in LES this will also influence the subgrid scales. The dynamic Smagorinsky model is an isotropic model, in the sense that the SGS viscosity ν_{SGS} is direction independent. In the same spirit as Reynolds stress-based models for RANS, the model here discussed is called the explicit algebraic SGS stress model (EAM). The EAM was developed by Marstorp [14] and is similar to the explicit algebraic Reynolds stress model (EARSM) by Wallin and Johansson [21]. The EAM is based on a modeled transport equation of the SGS stresses and on the assumption that the advection and diffusion of the SGS stress anisotropy are negligible. The model formulation is given by

$$\tau_{ij} = \frac{2}{3}\delta_{ij} K_{\mathrm{SGS}} + \underbrace{\beta_1 K_{\mathrm{SGS}}}_{\text{eddy viscosity}} \widetilde{S}^*_{ij} + \underbrace{\beta_4 K_{\mathrm{SGS}} (\widetilde{S}^*_{ik}\widetilde{\Omega}^*_{kj} - \widetilde{\Omega}^*_{ik}\widetilde{S}^*_{kj})}_{\text{nonlinear contribution}}. \tag{3}$$

where $\widetilde{S}^*_{ij}$ and $\widetilde{\Omega}^*_{ij}$ are the filtered strain and rotation-rate tensors normalized by $1/\tau^*$, the inverse of the SGS turbulence time scale. The second term on the right-hand side is an eddy viscosity term responsible for SGS dissipation, whereas the third term accounts for anisotropic effects of SGS stresses and models the disalignment of the SGS stress and resolved strain-rate tensor. The β_1 and β_4 coefficients are given by

$$\beta_1 = -\frac{33}{20}\frac{9c_1/4}{[(9c_1/4)^2 + |\widetilde{\Omega}^*|^2]}, \quad \beta_4 = -\frac{33}{20}\frac{1}{[(9c_1/4)^2 + |\widetilde{\Omega}^*|^2]}, \tag{4}$$

where $|\widetilde{\Omega}^*| = (2\tau^{*^2}\widetilde{\Omega}_{ij}\widetilde{\Omega}_{ij})^{1/2}$ and $\widetilde{\Omega}_{ij}$ is the filtered rotation-rate tensor. The unknown quantities K_{SGS} and τ^* can be dynamically or nondynamically computed. The dynamic version of the EAM involves Germano's dynamic procedure. Here the SGS kinetic energy is modeled in terms of the squared Smagorinsky velocity scale $\Delta|\widetilde{S}|$ [22],

$$K_{\mathrm{SGS}} = c\widetilde{\Delta}^2|\widetilde{S}|^2, \tag{5}$$

where $\widetilde{\Delta} = \sqrt[3]{\Omega}$ is the filter scale based on Ω, the volume of a computational cell, $|\widetilde{S}| = (2\widetilde{S}_{ij}\widetilde{S}_{ij})^{1/2}$, and c is a dynamic parameter, computed in the following way:

$$c = \frac{1}{2}\frac{\langle \widehat{\widetilde{u}_i \widetilde{u}_i} - \widehat{\widetilde{u}_i}\widehat{\widetilde{u}_i} \rangle}{\langle \widehat{\widetilde{\Delta}}^2 \widehat{\widetilde{S}}_{ij}\widehat{\widetilde{S}}_{ij} - \widetilde{\Delta}^2 \widehat{\widetilde{S}_{ij}\widetilde{S}_{ij}} \rangle}. \tag{6}$$

The quantities with $\widehat{\cdot}$ are test-filtered quantities and $\langle\cdot\rangle$ denotes a spanwise average. Here we will use $\widehat{\widetilde{\Delta}} = 2\widetilde{\Delta}$.

The expression for c is a direct consequence of EAM SGS formulation. In contrast to EAM, the expression comes from the scale similarity of the SGS stress tensor. As a consequence in the EAM one needs to compute fewer terms in the dynamic procedure.

Once c is computed, it is possible to obtain the coefficient c_1 and the SGS time scale τ^*, which according to [14] are given by

$$c_1 = c_1'\sqrt{c_3'}\frac{c^{1.25}}{(2C_s)^{2.5}}, \quad \tau^* = c_3'\frac{1.5C_k^{1.5}\sqrt{c}}{2C_s}|\widetilde{S}|^{-1}, \tag{7}$$

where $c_1' = 3.12$, $c_3' = 0.91$, $C_k = 1.5$ is the Kolmogorov constant and $C_s = 0.1$.

In addition to [14], the SGS timescale value has been locally bounded from below with the Kolmogorov timescale near the wall, τ_η, which reads

$$\tau_\eta \approx 2\frac{\nu}{u_\tau^2} = \tau^*_{\min}. \tag{8}$$

The model is not sensitive to the exact choice of $\tau^*_{\min}$.

Furthermore, c_1 has been limited to larger values than 0.27 and the wall-normal SGS stress component has been limited to non-negative values, i.e., $\tau_{22} \geqslant 0$.

1. The role of anisotropy in EAM

In this section, we investigate the impact of the anisotropic contribution to the SGS stress tensor, τ_{ij}, in turbulent channel flow at friction Reynolds numbers of 550, 2000, and 5200. Details of the LESs are presented in the next section. We denote the third term of equation (3), $\tau_{ij,\text{nlin}}$, and the sum of the two first ones,$\tau_{ij,\text{lin}}$. As seen from expression (3), the nonlinear part, $\tau_{ij,\text{nlin}}$, gives the largest contribution to the streamwise and wall-normal diagonal components of the Reynolds stress tensor, with a maximum peak in proximity of the wall [see Figs. 1(a) and 1(b)]. For the streamwise component, $\tau_{11,\text{nlin}}$ increases the peak close to the wall, to about twice its value obtained with $\tau_{11,\text{lin}}$ only. This results in a total Reynolds stress, R_{uu}, with a peak that is very close to DNS values, as we will see later. For the wall-normal component, instead, $\tau_{22,\text{nlin}}$ counteracts $\tau_{22,\text{lin}}$ near the wall, which otherwise would be largely overpredicted. $\tau_{12,\text{nlin}}$ also modifies the shear stress [Fig. 1(c)] component of the SGS stress, and improves the resulting prediction. For all components $\tau_{ij,\text{nlin}}$ is concentrated much closer to the wall than $\tau_{ij,\text{lin}}$. This is natural since the anisotropy of the stresses becomes very large there. Moreover, since the range of scales decreases near the wall, more of the anisotropy must be captured by the SGS model. The dynamic Smagorinsky SGS contribution to the shear stress is usually not sufficiently large in order to predict a correct Reynolds shear stress peak. The contribution of anisotropy is negligible for the third diagonal term and the other deviatoric terms.

Figure 2 shows that the influence of the Reynolds number on $\tau_{ij,\text{nlin}}$ is quite small. The influence of $\tau_{ij,\text{nlin}}$ is essentially restricted to the viscous sublayer and the buffer region for all Re_τ with a slightly increasing amplitude with increasing Re_τ.

III. NUMERICAL SETUP OF THE LES

To perform LES of fully developed turbulent channel flow, the SIMSON code [23] was used. The homogeneous streamwise x and spanwise z directions were discretized using Fourier series and the wall-normal y direction using Chebyshev polynomials. The solution is dealiased in the wall-parallel directions. The EAM and the DSM were used.

The computational box is $L_x = 5\pi\delta$ and $L_z = 2\pi\delta$ in streamwise and spanwise directions respectively, where δ is the channel half-width. DNS reference data were used from [24] for box size $L_x = 8\pi\delta$, $L_z = 4\pi\delta$ and $\text{Re}_\tau \approx 550$, box size $L_x = 8\pi\delta$, $L_z = 3\pi\delta$ and $\text{Re}_\tau \approx 2000$; and from [13] for box size $L_x = 8\pi\delta$, $L_z = 3\pi\delta$ and $\text{Re}_\tau \approx 5200$.

The computational domain of the LES is somewhat smaller than that of the DNS to reduce computational costs, but it is still large enough to capture the large-scale structures, as will be shown later.

The LESs are run with a constant mass flow rate. We enforce the LESs to have the same bulk Reynolds number as the reference DNS. This implies that in general Re_τ and the skin friction coefficient of the LESs deviate from these of the corresponding DNS.

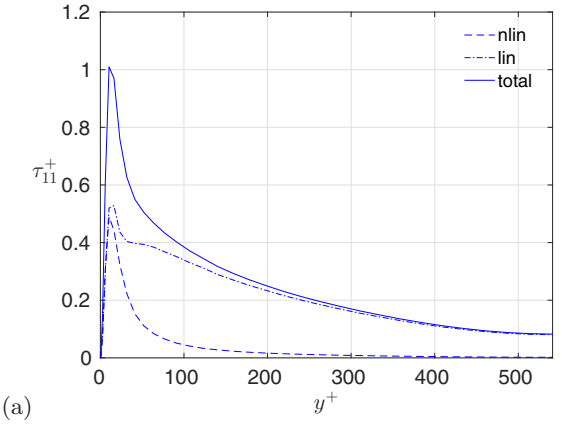

(a)

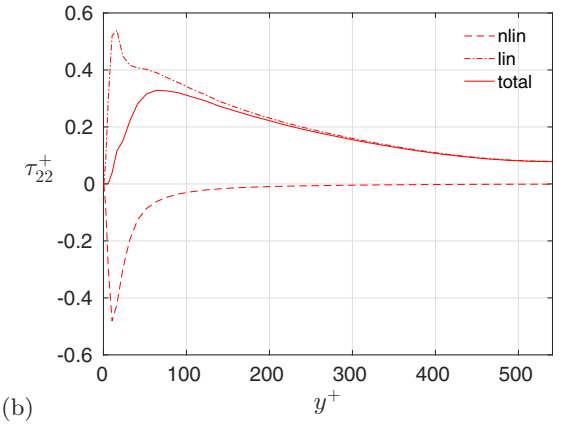

(b)

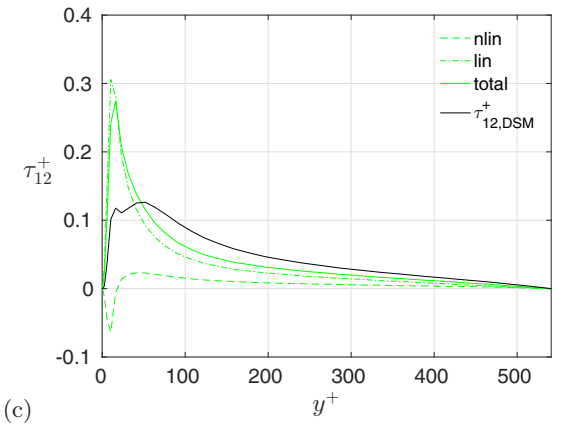

(c)

FIG. 1. Non-linear (nlin) and linear (lin) parts of τ_{11} (a), τ_{22} (b), τ_{12} (c) as a function of the wall-normal direction in wall units. $\mathrm{Re}_\tau = 550$ and resolution according to EA550 in Table I.

The simulation parameters such as the resolution and the grid spacings Δx^+, Δy^+, Δz^+ in streamwise, wall-normal, and spanwise directions, respectively, in wall units, are shown in Table I. The LESs at the lowest Reynolds number are carried out at three different resolutions while the

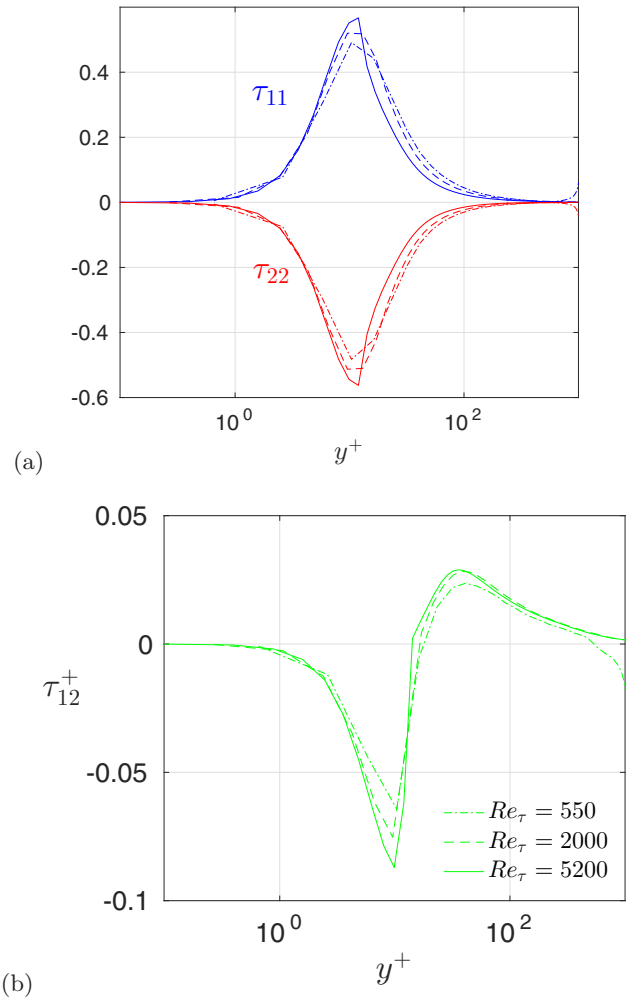

FIG. 2. Non-linear (nlin) parts of τ_{11}, τ_{22} (a), τ_{12} (b) as a function of the wall-normal direction in wall units, for $\mathrm{Re}_\tau = 550$ (dashed-dotted lines), $\mathrm{Re}_\tau = 2000$ (dashed lines) and $\mathrm{Re}_\tau = 5200$ (full lines). Resolution according to EA550, EA2000 and EA5200 in Table I.

LESs at the higher Reynolds numbers are carried out at two resolutions. We will call the LESs with the coarse resolution of $\Delta x^+ \approx 150$ and $\Delta z^+ \approx 60$ (cases DS/EA550, DS/EA2000, DS/EA5200) cLES and LESs with the very coarse resolution of $\Delta x^+ \approx 250$ and $\Delta z^+ \approx 100$ (cases DS/EA550lr, DS/EA2000lr, DS/EA5200lr) vcLES. The LESs at the lowest Reynolds number and $\Delta x^+ \approx 67$ and $\Delta z^+ \approx 27$ are called fLES.

IV. RESULTS

In the following section we will assess the performance of the EAM and DSM in LES at resolutions that go from the normal/fine resolutions to very coarse resolutions (see Table I). We start with basic quantities such as skin friction coefficient, mean velocity profiles, and Reynolds stresses. Anisotropy invariants are also used to compare the LESs. Finally, an analysis of the prediction of large-scale structures has been performed using energy spectra.

TABLE I. Channel flow simulations, from $\mathrm{Re}_\tau \approx 550$ up to $\mathrm{Re}_\tau \approx 5200$. N_x, N_y, N_z are the numbers of Fourier modes and Chebychev polynomials in the streamwise, wall-normal, and spanwise directions, respectively. Δy_w^+ and Δy_c^+ are the grid spacings in wall-normal direction at the wall and at the channel flow centreline ($*$ and $**$ by [24] and $***$ from [13]).

Case	SGS model	$N_x \times N_y \times N_z$	Δx^+	Δz^+	Δy_w^+–Δy_c^+	Re_τ
DS550lr	DSM	$32 \times 65 \times 32$	270	108	0.66–26.99	461
EA550lr	EAM	$32 \times 65 \times 32$	270	108	0.66–26.99	516
DS550	DSM	$60 \times 65 \times 60$	144	58	0.66–26.99	503
EA550	EAM	$60 \times 65 \times 60$	144	58	0.66–26.99	541
DS550hr	DSM	$128 \times 65 \times 128$	67	27	0.66–26.99	528
EA550hr	EAM	$128 \times 65 \times 128$	67	27	0.66–26.99	549
DS2000lr	DSM	$128 \times 193 \times 128$	245	98	0.29–32.72	1784
EA2000lr	EAM	$128 \times 193 \times 128$	245	98	0.29–32.72	1935
DS2000	DSM	$200 \times 193 \times 200$	157	63	0.29–32.72	1873
EA2000	EAM	$200 \times 193 \times 200$	157	63	0.29–32.72	1991
DS5200lr	DSM	$320 \times 513 \times 320$	255	102	0.1–31.91	4693
EA5200lr	EAM	$320 \times 513 \times 320$	255	102	0.1–31.91	5129
DS5200	DSM	$512 \times 513 \times 512$	159	64	0.1–31.91	4914
EA5200	EAM	$512 \times 513 \times 512$	159	64	0.1–31.91	5231
DNS550*	DNS	$1024 \times 257 \times 1024$	13.4	6.7	$\Delta y^+_{\max} = 6.7$	547
DNS2000**	DNS	$4096 \times 633 \times 3072$	12.3	6.1	$\Delta y^+_{\max} = 8.9$	2003
DNS5200***	DNS	$10240 \times 1536 \times 7680$	12.7	6.4	0.498–10.3	5186

A. Skin friction coefficient

A proper estimation of the pressure gradient and related skin friction in a channel flow is an important and basic requirement for the LESs. In Fig. 3 the skin friction coefficient is shown as a function of the friction Reynolds number and is scaled with the corresponding DNS value. Note that the skin friction coefficient is based on the bulk velocity u_b.

The C_f of cLES with the EAM are within 98% of the DNS while the vcLES deviates 10% at $\mathrm{Re}_\tau = 550$ but this deviation decreases to 2% at $\mathrm{Re}_\tau = 5200$. The simulations with the DSM show much larger differences. In the cLES the differences with the DNS are 10% or larger and in the vcLES the differences are more than 20%. Only in the fLES does it come closer, although the difference

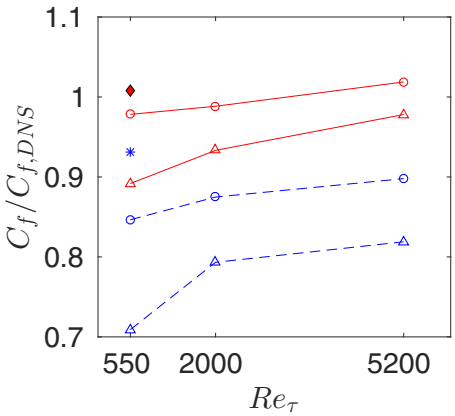

FIG. 3. Friction coefficient ratio between LES and DNS. Blue dashed line values refer to DSM, red straight line to EAM. △: vcLESs. ◯: cLESs. ∗: fLES-DSM. ♢: fLES-EAM.

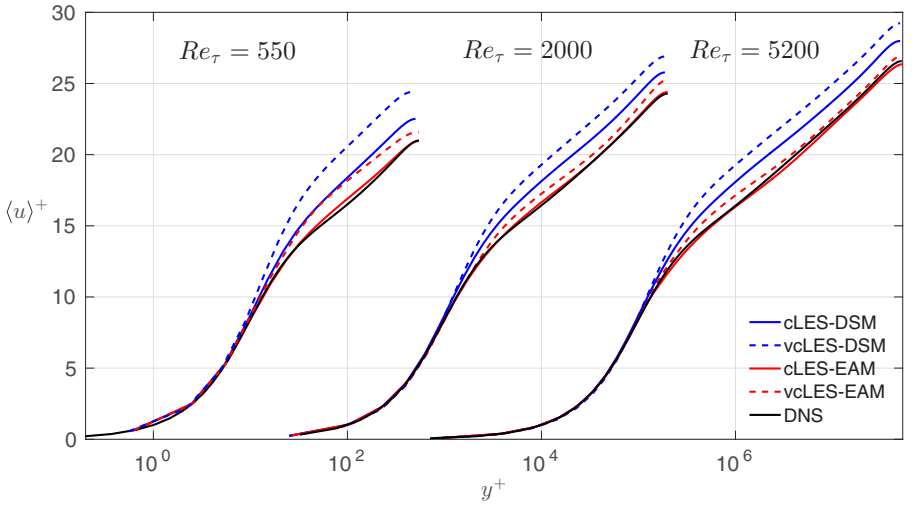

FIG. 4. Mean streamwise velocity in wall units, as a function of the viscous-scaled wall-normal direction. The three Re_τ cases are shifted by a factor of 10^2 viscous units, along the wall-normal coordinate.

with the DNS is still 7% whereas the fLES with the EAM agrees almost exactly with DNS. Except for the cLES with the EAM, we see that in general the agreement with the DNS becomes better at higher Re_τ, as previously shown in Ref. [17].

A possible explanation is that the large-scale turbulent structures become more important with Re_τ [25] and contribute more to the skin friction, while the smaller near-wall structures, which are likely less well represented in the cLES and vcLES, become less important. The implication is that the resolution requirements become less severe at higher Reynolds numbers.

B. Mean velocity

Velocity profiles in wall units, for $\mathrm{Re}_\tau = 550$, 2000, and 5200, are shown in Fig. 4. Very close to the wall, the behavior of LES with both models is mostly dominated by viscous effects, which require a wall-normal resolution in the order of $y^+ = 1$.

Differences between the LESs with the two models are substantial and are illustrated by the shift in the logarithmic layer. The cLES with the EAM gives an accurate description of the velocity profile, while the vcLES has a slight overprediction of the velocity in the outer layer, which becomes less with increasing Reynolds number. This overprediction is much smaller than the one given by the LES with DSM at the same resolution. Only in the fLES with the DSM is the agreement with DNS fairly good (not shown here).

The high degree of independence of resolution and Reynolds number in the LES with EAM for the mean velocity profiles can probably be explained by the better description of anisotropy near the wall, which is substantial at coarse resolutions.

C. Reynolds stresses

The Reynolds stresses are the sum of the resolved and SGS stresses which are available from the EAM. In case of the DSM, the normal SGS stresses are basically isotropic and directly related to K^{SGS}, but since K^{SGS} is not available, for DSM the Reynolds stresses are only the resolved stresses.

Figures 5(a) and 5(b) show profiles of the streamwise component of the Reynolds stress tensor for $\mathrm{Re}_\tau = 550$ and $\mathrm{Re}_\tau = 5200$, respectively.

The difference between the LESs with the two models is noticeable, particularly in the buffer layer. The high Reynolds stress, given by the vcLES with DSM, illustrates how the DSM largely

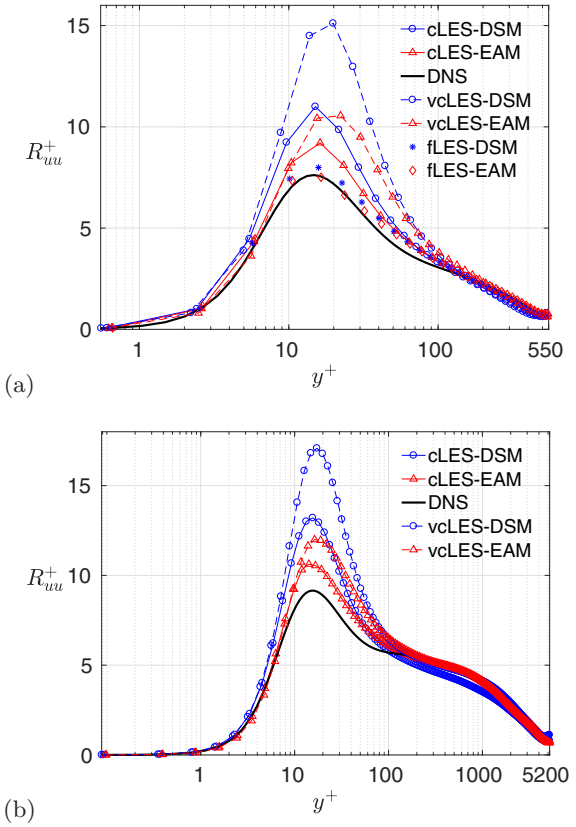

FIG. 5. Total streamwise Reynolds stress components at (a) $\mathrm{Re}_\tau = 550$ and (b) $\mathrm{Re}_\tau = 5200$.

overestimates the streamwise Reynolds stress component if the mesh is not sufficiently fine. LES with DSM, in fact, achieves a similar solution as with EAM only when the resolution is doubled. Using a fine resolution [Fig. 5(a)], the DNS peak is well captured by fLES with EAM and with 15% error with cLES. Hence, in order to get reliable results, LES with EAM requires a substantially lower number of grid points than LES with DSM.

In Figs. 6 and 7 we show the SGS contribution to the Reynolds stresses by cLESs at $\mathrm{Re}_\tau = 550$ and $\mathrm{Re}_\tau = 5200$, respectively. Both the total Reynolds stress tensor components and their SGS parts are shown.

In Fig. 6 we note that the cLES with DSM overpredicts the streamwise component and underpredicts the wall-normal component of Reynolds stress (with about 40% in peak magnitude). Also the spanwise component is substantially underpredicted with DSM. The underprediction to some extent can be explained by the missing SGS part, although the overpredicted streamwise component will be even higher if this part is included. cLES with the EAM, on the other hand, gives a much more realistic distribution of the energy among the different normal components reasonably close to the DNS results for both Reynolds numbers. In particular the prediction in the inner layer is substantially improved. Note also the difference in magnitude of the SGS contribution for the different components [26].

Reynolds shear stress is well computed by cLES with the both models. However, a close-up of the inner layer peak reveals a slight underestimation by cLES with DSM. With a two times larger magnitude of the SGS contribution, cLES with EAM comes closer to the DNS. It has been observed that this misprediction decreases in LES as the Reynolds number is increased. This is visible in the near-wall close-up, shown in Fig. 8. We here see the Reynolds shear stress behavior for the two

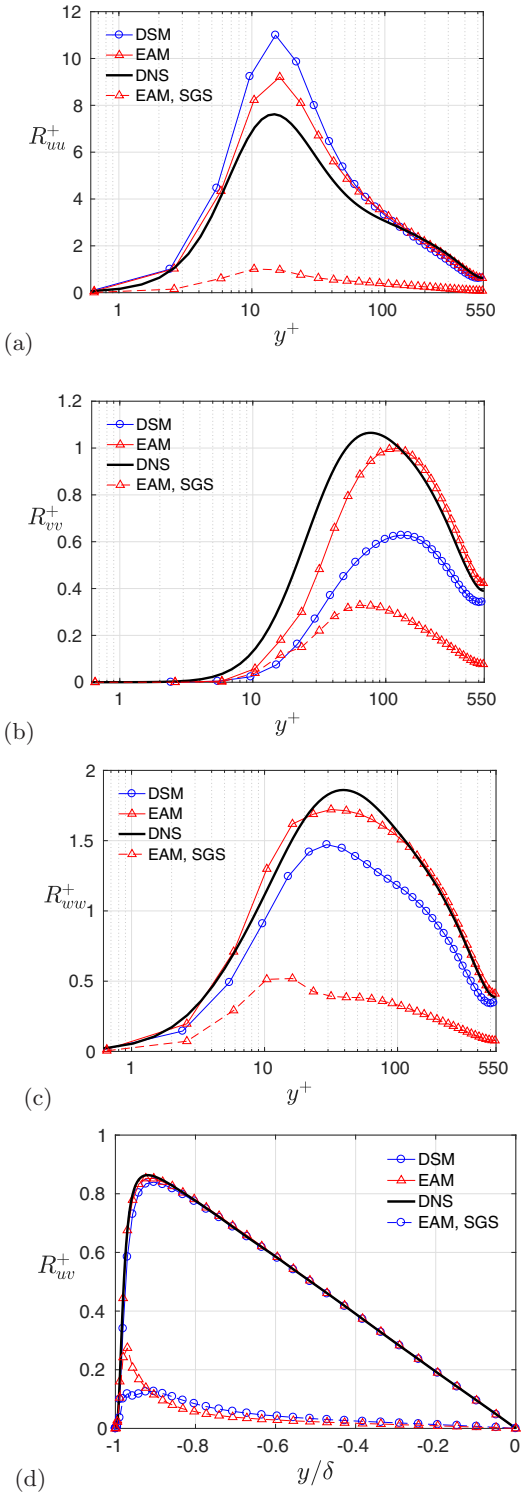

FIG. 6. Total and SGS parts of (a) streamwise, (b) wall-normal, (c) spanwise Reynolds stress components and (d) Reynolds shear stress by cLES at $\mathrm{Re}_\tau = 550$. In (a)–(c) DSM represents the resolved part only.

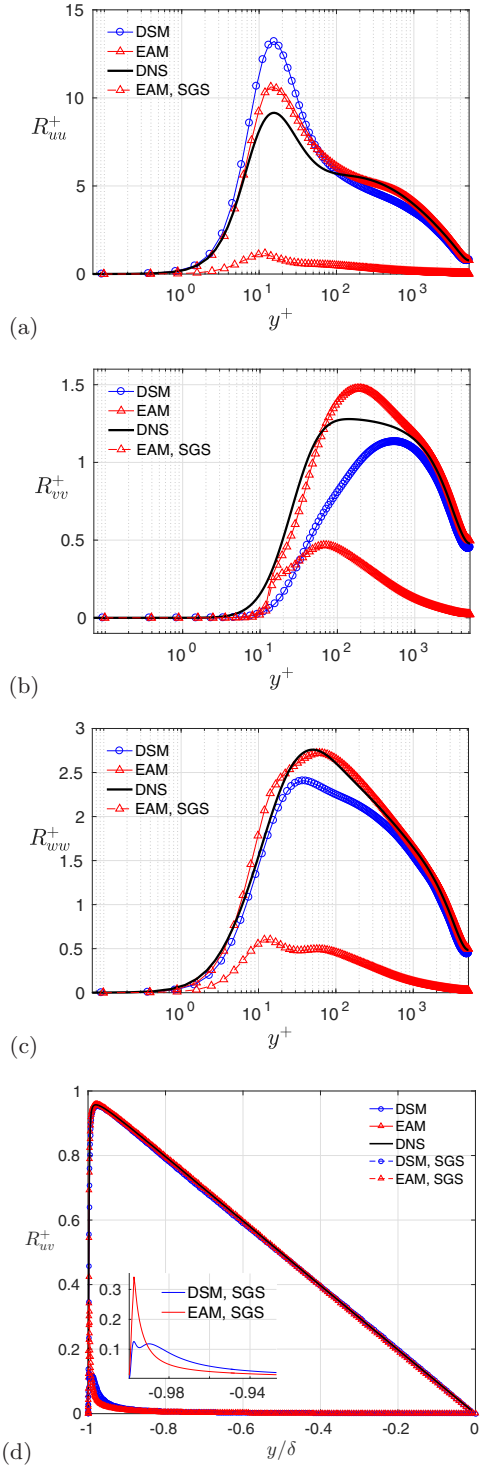

FIG. 7. Total and SGS parts of (a) streamwise, (b) wall-normal, (c) spanwise Reynolds stress components and (d) Reynolds shear stress by cLES at $\mathrm{Re}_\tau = 5200$ with a close-up of the SGS contributions. In (a)–(c) DSM represents the resolved part only.

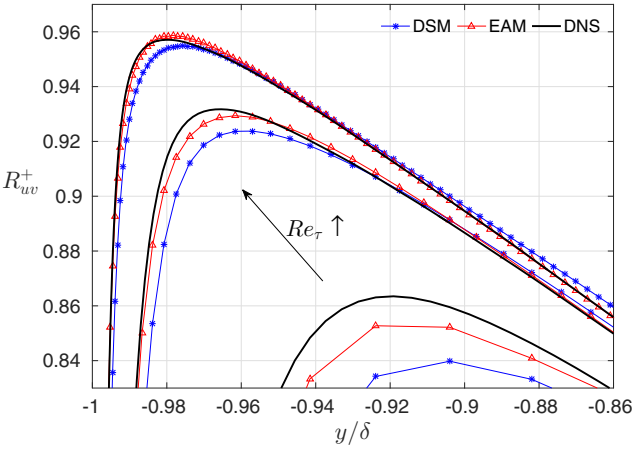

FIG. 8. Close-up of the Reynolds shear stress peaks by cLES, for $\mathrm{Re}_\tau = 550$, 2000, and 5200 as a function of the wall-normal direction. The arrow points in the increasing Re_τ direction.

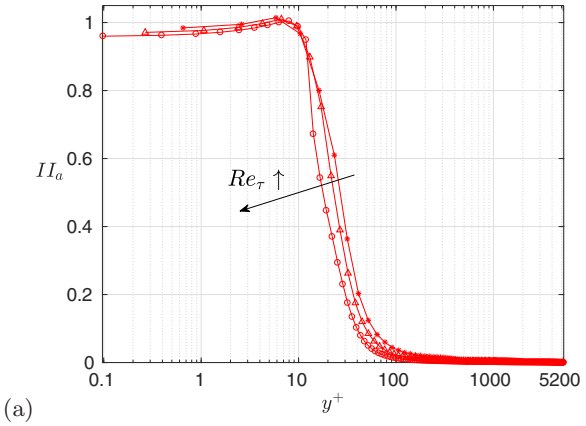

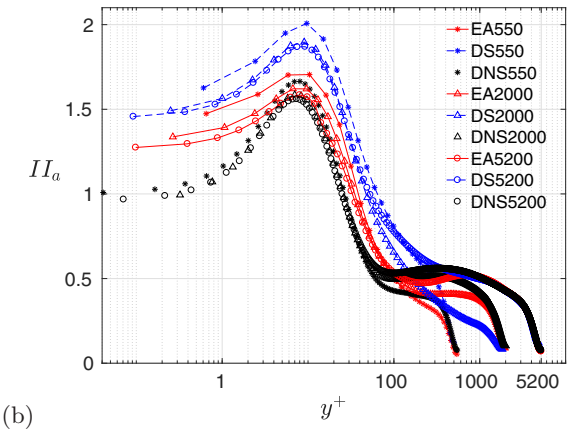

FIG. 9. (a) II_a^{SGS} and (b) II_a for cLES with EAM (red lines), cLES with DSM (blue lines), and DNS (black lines), at $\mathrm{Re}_\tau = 550$, 2000, and 5200.

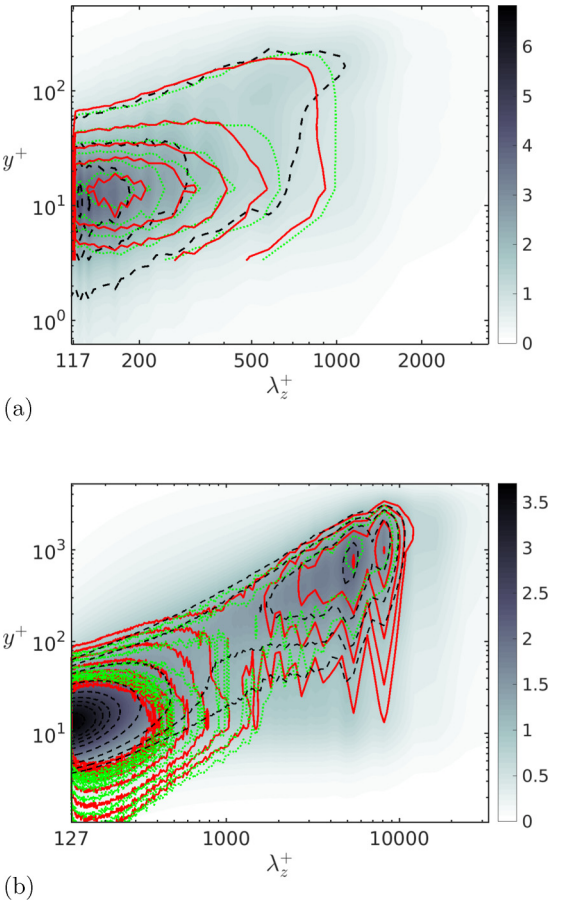

FIG. 10. Premultiplied spanwise energy spectra $k_z E_{uu}^{1D}/u_\tau^2$ of the streamwise velocity as a function of the spanwise wavelength λ_z^+ and wall distance y^+. cLES with DSM ($\cdots$, green), cLES with EAM (–, red), and DNS (– –, black) data, at $\mathrm{Re}_\tau = 550$ (a) and $\mathrm{Re}_\tau = 5200$ (b). DNS contour plot in the background.

models for three friction Reynolds numbers. Regardless of the Reynolds number, cLES with the DSM is not able to predict the peaks in an accurate way. On the other hand, cLES with EAM has its maximum SGS contribution in the region near the wall, and that gives a more correct behavior of the peaks near the wall. In addition, it has been seen that EAM's accuracy increases with Re_τ. A possible reason was discussed above. For high Reynolds numbers, large scale motions will contribute more to the total kinetic energy.

D. Anisotropy invariants

The main feature of the EAM is to properly reproduce anisotropy of wall-bounded flows. An important question is how much the modeled SGS anisotropy varies with Reynolds numbers. In order to evaluate the SGS model influence, we use the SGS anisotropy and total anisotropy defined as

$$a_{ij}^{\mathrm{SGS}} = \frac{\langle \tau_{ij} \rangle}{\langle K_{\mathrm{SGS}} \rangle} - \frac{2}{3}\delta_{ij}, \quad a_{ij} = \frac{\langle \widetilde{u}_i \widetilde{u}_j \rangle + \langle \tau_{ij} \rangle}{K_{\mathrm{RES}} + \langle K_{\mathrm{SGS}} \rangle} - \frac{2}{3}\delta_{ij} \tag{9}$$

where $K_{\mathrm{SGS}} = \tau_{kk}/2$ and $K_{\mathrm{RES}} = \langle \widetilde{u}_k \widetilde{u}_k \rangle/2$ are the SGS and resolved parts of the turbulence kinetic energy, respectively, and $\langle \cdot \rangle$ is the plane and time average. In order to quantify the anisotropy, we

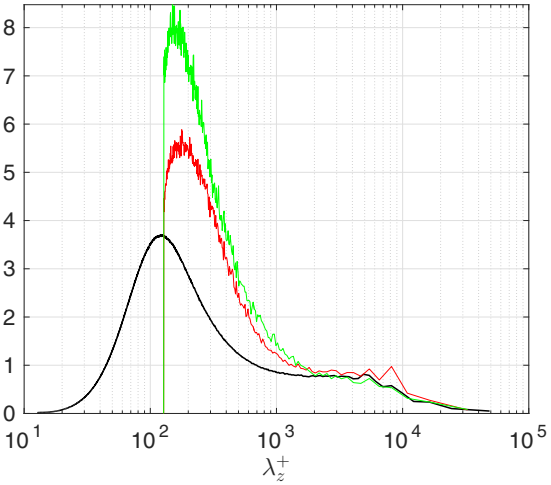

FIG. 11. Premultiplied spanwise energy spectra $k_z E_{uu}^{1D}/u_\tau^2$ of the streamwise velocity as a function of the spanwise wave length λ_z^+ at $y^+ \approx 15$, for $\mathrm{Re}_\tau = 5200$. cLES with DSM (green), cLES with EAM (red), and DNS (black) data.

focus on the magnitude given by the second invariant of anisotropy,

$$II_a^{\mathrm{SGS}} = a_{ij}^{\mathrm{SGS}} a_{ji}^{\mathrm{SGS}}, \quad II_a = a_{ij} a_{ji} \tag{10}$$

for the corresponding SGS and total parts. The SGS anisotropy invariant can only be obtained for the EAM. In Fig. 9(a) we note that II_a^{SGS} is significant only in the viscous sublayer and buffer region, and decreases rapidly outside this region. It signifies a SGS state that is close to a two-component limit in the near-wall region. Here, the range of scales decreases, thus anisotropy persists down to the subgrid scales. The SGS anisotropy is sensitive to Reynolds numbers only in the buffer layer, with high anisotropy being restricted to a smaller region (in wall units) for higher Reynolds number. The reason for the Re dependency is not completely clear, but is likely due to the difference in resolution in the y direction in this region (due to clustering of points near the wall related to the use of Chebychev polynomials) which will influence the filter width ($\Delta = \sqrt[3]{\Delta x \Delta y \Delta z}$).

The second invariants based on the total Reynolds stress, II_a, for the EAM and the DSM are compared to DNS data in Fig. 9(b). DNS shows a small decrease of II_a with increasing Reynolds number in the inner layer. In the buffer layer, a Reynolds number dependency is noticeable only in the inner peak region. Going further from the wall, the extension of the logarithmic region grows with increasing Reynolds number, and there the anisotropy establishes a plateau. Note that the interval at which the SGS anisotropy [Fig. 9(a)] shows a dependency with the Reynolds number, corresponds to the inner peak location of II_a. Except for the inner sublayer with $y^+ \lesssim 1$ where the intensity levels are very low, EAM gives a correct level of SGS anisotropy, unlike the DSM.

For the resolved part, the cLES with the DSM gives a large overprediction in the inner part and a substantial misprediction also in the outer region. The DSM exhibits a large overprediction of anisotropy of y^+ at least up to 100.

The cLES with the EAM gives results close to DNS from the buffer layer up to the outer region, for all Reynolds numbers. The magnitude of the inner peak is very near to that for the DNS.

E. Energy spectra

In order to assess the influence of the SGS models on the description of large scale turbulent structures we consider spanwise one-dimensional premultipled energy spectra of the streamwise velocity as function of the wall-distance at $\mathrm{Re}_\tau = 550$ and 5200; see Fig. 10. At higher Re_τ we see

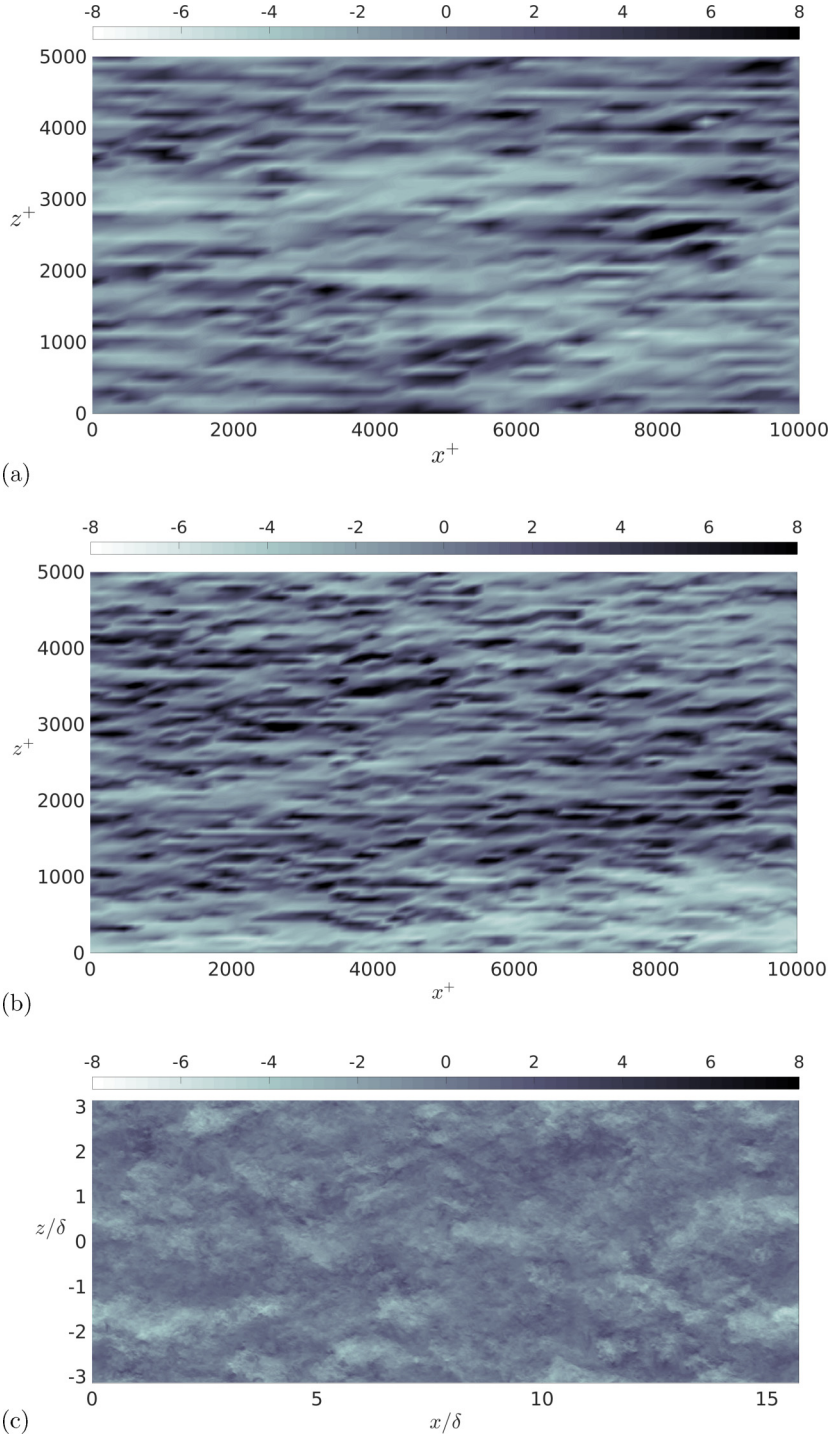

FIG. 12. Horizontal snapshots of the streamwise velocity fluctuations, normalized with the friction velocity u_τ. (a), (b) Planes at $y^+ \approx 10$ showing only a fraction (2%) of the computational domain, and (c) at $y^+ \approx 750$ showing the complete domain. (a) vcLES-EAM; (b), (c) cLES-EAM.

clearly more energetic large-scale structures in the cLES and a larger scale separation between the near-wall and outer structures.

For the outer scales at $\mathrm{Re}_\tau = 550$ the are some differences between DNS and both cLES, but at the higher Reynolds number the cLES with the EAM accurately captures the peak in the outer layer. The magnitude of the outer peak estimated by the cLES with DSM is slightly lower but also agrees quite well with DNS. The cLESs naturally gives inner layer structures that are wider than those obtained with DNS, since with a spanwise resolution of $\Delta z^+ \approx 60$ the streaks cannot be resolved. It follows that the cLES with EAM and DSM correctly predicts the scale and energy of the large-scale outer structures at higher Re_τ even if the near-wall structures are not completely correctly represented.

Figure 11 shows the premultiplied spanwise energy spectrum at $\mathrm{Re}_\tau = 5200$ at a position in the proximity of the inner peak, i.e., $y^+ \approx 15$. This once more illustrates that the streaks in the cLES are wider than in the DNS, but also shows that the near wall energy peak is close to the filter cutoff. In cLES both with the EAM and the DSM the energy peak is higher than in the DNS but in the case with the DSM the overprediction of energy is significantly larger than for the spectrum obtained with the EAM, which is directly related to the overprediction of u_{rms} with DSM.

F. Plane visualisations

Visualisations of the instantaneous streamwise fluctuations u'^+ along the xz plane near the wall, taken from vcLES-EAM and cLES-EAM are provided in Figs. 12(a) and 12(b). Note that only a small part (about 2%) of the domain is shown in the figure.

As expected, we observe that the resolution of the smallest near-wall structures improves moving from the very coarse to the coarse grid. In the cLES the streaks near the wall are more qualitatively captured, and are closer to the correct characteristic length scales of these structures, which are around $\lambda_x^+ \approx 1000$ and $\lambda_z^+ \approx 100$ [Fig. 12(b)] [27].

Figure 12(c) shows a horizontal snapshot of the streamwise fluctuations u'^+ in the entire xz plane, in proximity of the outer layer peak, using the coarse grid. In this visualisation we can see the imprints of the large-scale structures with a spanwise scale of $\sim h$ [see Fig. 10(b)]. The computation of the outer layer large-scale structures is less sensitive to the grid resolution. A very similar result is achieved using the very coarse resolution, resulting in essentially the same figure as 12(c).

V. CONCLUSIONS

The accuracy of LES with the EAM in prediction of wall-bounded flow has been investigated by performing a series of LESs of fully developed turbulent channel flow at three friction Reynolds numbers using three different resolutions ranging from quite fine to very coarse.

Skin friction coefficients are reasonably well captured by LES with EAM at all resolutions used, showing that the EAM gives much more resolution-independent results than the DSM, in agreement with [17]. Mean velocity profiles computed by LES with EAM exhibit a substantially better agreement with DNS than LES with DSM, for all the Reynolds number investigated, especially for coarse grids. The prediction of the Reynolds stress tensor components by LES with EAM are substantially improved compared to LES with DSM, and the peaks near the wall are substantially better predicted. In particular, the severe overprediction of the streamwise fluctuation intensity by LES with DSM has been considerably reduced using the EAM.

An analysis of the contributions to the stresses from the different parts of the SGS model reveals that the EAM prediction capability is strongly coupled to its ability of capturing anisotropy. The second invariant of the SGS anisotropy shows that the magnitude of the SGS anisotropy is large at all Reynolds numbers in the near-wall region. Near-wall physics are better reproduced if this anisotropy is accounted for in the SGS model.

As the Reynolds number increases, large-scale turbulent structures become a more dominant feature in the outer layer turbulence. Energy spectra show that LES both with EAM and DSM accurately predict the large-scale outer layer structures at higher Reynolds numbers even when the

resolution is not sufficient to predict near-wall structures correctly. In the buffer region the DSM gives a larger overprediction of the energy of the scales typical of streaks than the EAM.

The ability of EAM to substantially improve LES predictions at coarse resolutions indicates that LES with EAM can take LES of wall-bounded turbulent flows to substantially higher Reynolds numbers and can possibly (with further improvements) be an alternative to wall-modeled LES (WMLES).

ACKNOWLEDGMENTS

Support from the Swedish Research Council through Grants No. 621-2014-5700 and No. 621-2013-5784 and computer time provided by the Swedish National Infrastructure for Computing (SNIC) are gratefully acknowledged.

[1] H. Choi and P. Moin, Grid-point requirements for large eddy simulation: Chapman's estimates revisited, Phys. Fluids **24**, 011702 (2012).
[2] P. Sagaut, *Large Eddy Simulation for Incompressible Flows: An Introduction* (Springer, New York, 2006).
[3] U. Piomelli and E. Balaras, Wall-layer models for large-eddy simulations, Annu. Rev. Fluid Mech. **34**, 349 (2002).
[4] U. Piomelli, Wall-layer models for large-eddy simulations, Prog. Aerosp. Sci. **44**, 437 (2008).
[5] P. R. Spalart, Detached-eddy simulation, Annu. Rev. Fluid Mech. **41**, 181 (2009).
[6] U. Piomelli, Large eddy simulations in 2030 and beyond, Philos. Trans. R. Soc. London A **372**, 20130320 (2014).
[7] C. Mockett, M. Fuchs, and F. Thiele, Progress in DES for wall-modelled LES of complex internal flows, Comput. Fluids **65**, 44 (2012).
[8] J. Larsson, S. Kawai, J. Bodart, and I. Bermejo-Moreno, Large eddy simulation with modeled wall-stress: Recent progress and future directions, Mech. Eng. Rev. **3**, 15-00418 (2016).
[9] J. Fröhlich and D. von Terzi, Hybrid LES/RANS methods for the simulation of turbulent flows, Prog. Aerosp. Sci. **44**, 349 (2008).
[10] M. L. Shur, P. R. Spalart, M. K. Strelets, and A. K Travin, A hybrid RANS-LES approach with delayed-DES and wall-modelled LES capabilities, Int. J. Heat Fluid Flow **29**, 1638 (2008).
[11] M. Gritskevich, A. Garbaruk, and F. Menter, A comprehensive study of improved delayed detached eddy simulation with wall functions, Flow Turbul. Combust. **98**, 461 (2016).
[12] M. Germano, U. Piomelli, P. Moin, and W. H. Cabot, A dynamic subgrid-scale eddy viscosity model, Phys. Fluids **3**, 1760 (1991).
[13] M. Lee and R. D. Moser, Direct numerical simulation of turbulent channel flow up to $\mathrm{Re}_\tau \approx 5200$, J. Fluid Mech. **774**, 395 (2015).
[14] L. Marstorp, G. Brethouwer, O. Grundestam, and A. V. Johansson, Explicit algebraic subgrid stress models with application to rotating channel flow, J. Fluid Mech. **639**, 403 (2009).
[15] A. Rasam, S. Wallin, G. Brethouwer, and A. V. Johansson, Large eddy simulation of channel flow with and without periodic constrictions using the explicit algebraic subgrid-scale model, J. Turbul. **15**, 752 (2014).
[16] A. Rasam, G. Brethouwer, and A. V. Johansson, An explicit algebraic model for the subgrid-scale passive scalar flux, J. Fluid Mech. **721**, 541 (2013).
[17] A. Rasam, G. Brethouwer, P. Schlatter, Q. Li, and A. V. Johansson, Effects of modelling, resolution and anisotropy of subgrid-scales on large eddy simulations of channel flow, J. Turbul. **12**, N10 (2011).
[18] F. Kremer and C. Bogey, Large-eddy simulation of turbulent channel flow using relaxation filtering: Resolution requirement and Reynolds number effects, Comput. Fluids **116**, 17 (2015).
[19] U. Piomelli, A. Rouhi, and B. J. Geurts, A grid-independent length scale for large-eddy simulations, J. Fluid Mech. **766**, 499 (2015).
[20] In the following simulations the filter used by the authors commutes with the spatial and time derivative, such that the commutation error is negligible.

[21] S. Wallin and A. V. Johansson, An explicit algebraic Reynolds stress model for incompressible and compressible turbulent flows, J. Fluid Mech. **403**, 89 (2000).

[22] A. Yoshizawa, Statistical theory for compressible turbulent shear flows, with the application to subgrid modeling, Phys. Fluids **29**, 2152 (1986).

[23] M. Chevalier, P. Schlatter, A. Lundbladh, and D. S. Henningson, SIMSON: A pseudo-spectral solver for incompressible boundary layer flows, KTH technical report, 2007 (unpublished).

[24] S. Hoyas and J. Jiménez, Scaling of the velocity fluctuations in turbulent channels up to $\mathrm{Re}_\tau = 2003$, Phys. Fluids **18**, 011702 (2006).

[25] J. Monty, J. Stewart, R. Williams, and M. Chong, Large-scale features in turbulent pipe and channel flows, J. Fluid Mech. **589**, 147 (2007).

[26] The kink noticeable in Fig. 7 is connected to the reasonable bounding of c_1, for the physics of the slow pressure term, as discussed in Sec. II.

[27] N. Hutchins and I. Marusic, Evidence of very long meandering features in the logarithmic region of turbulent boundary layers, J. Fluid Mech. **579**, 1 (2007).